The effect of acoustic phonon confinement on the momentum and energy relaxation of hot carriers in quantum wires

1998 J. Phys.: Condens. Matter 10 6091

(http://iopscience.iop.org/0953-8984/10/27/010)

J. Phys.: Condens. Matter **10** (1998) 6091–6104. Printed in the UK PII: S0953-8984(98)91572-7

The effect of acoustic phonon confinement on the momentum and energy relaxation of hot carriers in quantum wires

A Svizhenko†, S Bandyopadhyay† and M A Stroscio‡

† Department of Electrical Engineering, University of Nebraska, Lincoln, NE 68588, USA
‡ US Army Research Office, PO Box 12211, Research Triangle Park, NC 27709, USA

Received 12 February 1998, in final form 22 April 1998

Abstract. The momentum and energy relaxation rates associated with electron–acoustic phonon interaction in a free-standing rectangular GaAs quantum wire have been calculated taking into account *confined* and *interface* phonon modes. Phonon confinement has two major consequences: (i) it increases relaxation rates by several orders of magnitude, and (ii) it increases the ratio of absorption to emission processes in narrow intervals of energy thereby making the energy relaxation rate in these intervals negative. An external magnetic field always decreases the momentum relaxation rate (thus increasing the carrier mobility) even though the scattering rate (the inverse of the quasi-particle lifetime) may increase or decrease depending on whether the interaction is polar (piezoelectric) or non-polar (deformation potential).

1. Introduction

Electron–phonon interaction in quantum wires has been studied by a number of researchers in the past [1–9, 11, 13]. In this paper, we present (to our knowledge) the first study of momentum and energy relaxation rates associated with such interactions when both electron and acoustic phonon confinement are taken into account. We also show how an external magnetic field can affect these rates.

The strength of electron–phonon interaction in a quantum wire depends on two quantities: the joint electron–phonon density of states, and the transition matrix element. Both of these quantities are influenced by quantum confinement of electrons and phonons. Phonon confinement causes significant non-linearities in the dispersion relations of acoustic phonon modes and vastly increases the phonon density of states. The electron density of states is also altered by quasi-one-dimensional confinement and (if a magnetic field is present) by the additional magnetostatic confinement due to the field [12]. As a result of the latter, the joint density of electron–phonon states depends on the magnetic field and can be 'tuned' using the field. The transition matrix element, on the other hand, is determined by the overlap between three entities: the wave function of the electron's initial state, the wave function of the final state, and a phonon's normal-mode amplitude. A magnetic field skews the wave functions of a travelling electron state towards an edge of the wire ('edge states'). This alters the overlap between the wave functions of the electron's initial state and final state and the phonon mode. Thus, it changes the transition matrix element. The combined result of all of this is that the scattering rate, the momentum relaxation rate and the energy relaxation rate are extremely sensitive to quantum confinement and the presence of an external magnetic field.

0953-8984/98/276091+14$19.50

This paper is organized as follows. In the next section we briefly present the prescription for calculating energy and momentum relaxation rates. Section 3 shows the results of our calculations, and the conclusions are presented in section 4.

2. Theory

The energy-dependent momentum and energy relaxation rates, $\tau_m^{-1}(E)$ and $\tau_e^{-1}(E)$, associated with any type of electron–phonon scattering are calculated from the corresponding transition rate $S(E_\nu, E'_{\nu'}, \pm\gamma, \pm\omega_\gamma)$ by integrating over all possible final electron states and phonon wave vectors, and then summing over all phonon modes or branches:

$$\frac{1}{\tau_m(E_\nu)} = \sum_n \int_0^\infty \int_0^{\gamma_{max}} \mathrm{d}E'_{\nu'}\ \mathrm{d}\gamma\ \ S(E_\nu, E'_{\nu'}, \pm\gamma, \pm\omega_{n,\gamma})(1 - f(E'_{\nu'}))\frac{(k - k')}{k} \tag{1}$$

$$\frac{1}{\tau_e(E_\nu)} = \sum_n \int_0^\infty \int_0^{\gamma_{max}} \mathrm{d}E'_{\nu'}\ \mathrm{d}\gamma\ \ S(E_\nu, E'_{\nu'}, \pm\gamma, \pm\omega_{n,\gamma})(1 - f(E'_{\nu'}))\frac{(E_\nu - E'_{\nu'})}{E_\nu} \tag{2}$$

where E_ν is the electron energy in the νth subband, k (γ) is the electron (phonon) wave vector along the unconfined direction of the quantum wire, $\omega_{n,\gamma}$ is the frequency of the nth phonon mode with wave vector γ, and $f(\eta)$ is the occupation probability of a state with energy η. Primed and unprimed quantities refer to initial and final electron states respectively. The calculation of the transition rate, $S(E_\nu, E'_{\nu'}, \pm\gamma, \pm\omega_{n,\gamma})$, for confined and interface acoustic phonon interaction in a quantum wire (subjected to a magnetic field) has been described by us in a previous paper [11]. The reader is referred to reference [11] for the pertinent technical details. We will assume that the electron distribution is non-degenerate so that $f(E'_{\nu'}) \approx 0$.

Equations (1) and (2) can be recast as

$$\frac{1}{\tau_m(E_\nu)} = \frac{1}{\hbar} \sum_{E_\nu - E'_{\nu'} \pm \hbar\omega_{n,\gamma} = 0} D^{\pm}(E'_{\nu'}, \omega_{n,\gamma})|M(E_\nu, E'_{\nu'})|^2(N + 1/2 \mp 1/2)\frac{(k - k')}{k} \tag{3}$$

$$\frac{1}{\tau_e(E_\nu)} = \frac{1}{\hbar} \sum_{E_\nu - E'_{\nu'} \pm \hbar\omega_{n,\gamma} = 0} D^{\pm}(E'_{\nu'}, \omega_{n,\gamma})|M(E_\nu, E'_{\nu'})|^2(N + 1/2 \mp 1/2)\frac{(E_\nu - E'_{\nu'})}{E_\nu} \tag{4}$$

where $M(E_\nu, E'_{\nu'})$ is the transition matrix element connecting initial and final electron states and $D^{\pm}(E'_{\nu'}, \omega_{n,\gamma})$ is the one-dimensional joint electron–phonon density of final states defined as

$$D^{\pm}(E'_{\nu'}, \omega_{n,\gamma}) = \frac{2\pi}{|\partial(E_\nu - E'_{\nu'} \pm \hbar\omega_{n,\gamma})/\partial\gamma|}\theta((E_\nu - E'_{\nu'} \pm \hbar\omega_{n,\gamma}) \tag{5}$$

with θ being the Heaviside unit step function. D^+ corresponds to phonon absorption and D^- corresponds to phonon emission. The summations in equations (3) and (4) are performed only over the zeros of the function $\phi^{\pm}_{n,\gamma,\nu} = E'_\nu(k \pm \gamma) - E_\nu(k) \mp \hbar\omega_{n,\gamma}$.

In order to obtain $D^{\pm}(E'_{\nu'}, \omega_{n,\gamma})$ and $M(E_\nu, E'_{\nu'})$, we start by first numerically solving the Schrödinger equation in a quantum wire subjected to a magnetic field to obtain the dispersion relations and wave functions of hybrid magnetoelectric states (see reference [12]). Next, we solve the elasticity equation numerically to derive the acoustic phonon modes and their dispersion relations (see reference [11]). In a quantum wire of rectangular cross-section, there are no exact solutions to the elasticity equation. Therefore, one can find only approximate solutions which have displacements along all three coordinate directions, unlike the pure shear, dilatational, and flexural modes of a quantum well [8–10]. From these results, we calculate $D^{\pm}(E'_{\nu'}, \omega_{n,\gamma})$ and $M(E_\nu, E'_{\nu'})$.

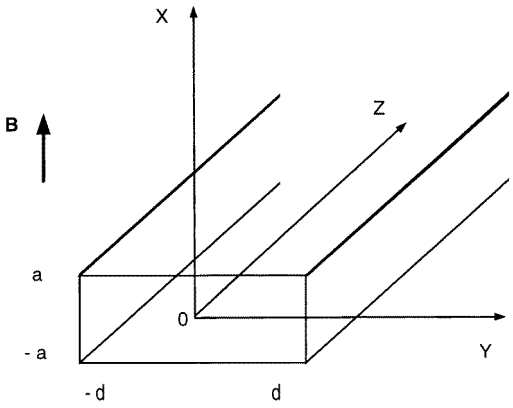

Figure 1. A quantum wire of rectangular cross-section subjected to a magnetic field along the x-axis. The width of the wire is much larger than the thickness.

3. Results

We have calculated the energy and momentum relaxation rates in a free-standing rectangular GaAs quantum wire of thickness 40 Å and width 500 Å (as shown in figure 1) with a magnetic field directed along the x-direction. The thickness (along the x-direction) is so small that only the lowest transverse subband in this direction will be occupied under all circumstances.

In figure 2, we plot the energy-conserving function $\phi^{\pm}_{n,\gamma,1} = E'_1(k \pm \gamma) - E_1(k) \mp \hbar\omega_\gamma$ as a function of the transfer wave vector $k' - k$ (or $\pm\gamma$) for the lowest four branches of the non-polar acoustic phonon 'thickness' modes [8, 9]. The solid lines correspond to absorption ($\phi^{+}_{n,\gamma,1} = E'_1(k + \gamma) - E_1(k) - \hbar\omega_\gamma$) and the broken lines to emission ($\phi^{-}_{n,\gamma,1} = E'_1(k - \gamma) - E_1(k) + \hbar\omega_\gamma$). No magnetic field is applied. The electron is in the lowest subband and has a kinetic energy $E_1 = 178.6$ meV. Note that we are considering only *intra-subband* scattering within the first electron subband. Zeros of the function ϕ correspond to simultaneous energy and momentum conservation and therefore the occurrence of a scattering event. In order to find the right phonon in the nth branch participating in a scattering event, we scan the phonon wave-vector space to locate the zeros of $\phi^{\pm}_{n,\gamma,\nu}$. This is easily accomplished by dividing the wave-vector space into a grid with a mesh spacing of $\Delta\gamma$ and then focusing on the regions where the product $\phi^{\pm}_{n,\gamma,\nu}\phi_{n,\gamma+\Delta\gamma,\nu}$ is negative.

We will now categorize scattering events into four categories: forward emission, forward absorption, backward emission, and backward absorption. 'Forward'-scattering processes will be defined as those which increase an electron's momentum by scattering it in the forward direction. Since the momentum increases, the quantity $k' - k$ is positive. For intra-subband transition *and* for scattering out of the lowest subband, forward scattering corresponds to absorption only, since emission will decrease the momentum. For inter-subband transitions, and when the initial state of the electron is not in the lowest subband, it could correspond to either absorption or emission. By the same token, we will define 'backward'-scattering events as those that decrease an electron's momentum by scattering it backward. For such a process, the quantity $k' - k$ is negative. In the case of both intra- and inter-subband transition, backscattering can correspond to either emission or absorption. The regions corresponding to forward absorption, backward emission, and backward absorption are shown in figure 2. Note that there is no region corresponding to forward emission since

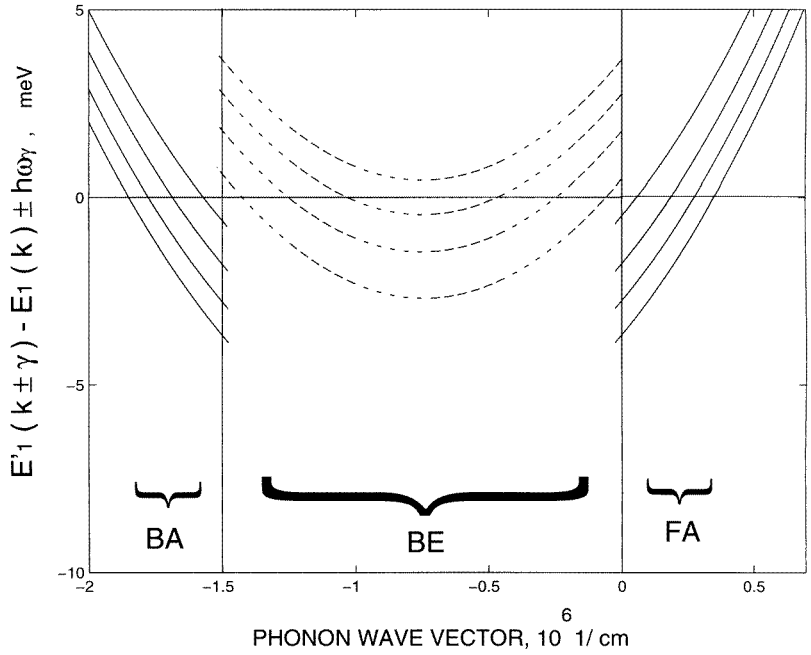

Figure 2. The energy- and momentum-conserving function $\phi^{\pm}_{n,\gamma,1} = E'_1(k \pm \gamma) - E_1(k) \mp \hbar\omega_{n,\gamma}$ for a GaAs quantum wire with thickness 28.3 Å and width 56.6 Å at zero magnetic field. The electron is initially in the lowest subband with an energy of 178.6 meV. Only intra-subband scattering is considered. The regions corresponding to forward absorption, backward emission, and backward absorption are designated. For intra-subband scattering, there can be no forward emission. Absorption is denoted by solid lines and emission by broken lines. Only the first four thickness branches of confined acoustic phonon modes are considered for clarity. Scattering takes place *only* when $\phi^{\pm}_{n,\gamma,1} = 0$.

(i) it is forbidden in intra-subband transition, and also (ii) it is forbidden when the initial state of the electron is in the lowest subband.

In figure 3, we plot the joint electron phonon density of states (JEPDS) (defined as $\text{JEPDS}^{\pm} = \sum_n D^{\pm}(E'_{v'}, \omega_{n,\gamma})$) as a function of the final electron energy E'_1 when the electron's initial state is in the first subband and its kinetic energy is $E_1 = 178.6$ meV. The lattice temperature is assumed to be 77 K. No magnetic field is applied. Again, only intra-subband scattering is considered, but all width and thickness modes of acoustic phonons (within a phonon energy of $10kT$) are taken into account in the summation for $\text{JEPDS}^{\pm}$. There are a denumerably infinite number of confined phonon modes, but the higher-energy modes are barely occupied because the occupation probability is governed by Bose–Einstein statistics. The solid line in figure 3 corresponds to backward phonon absorption and the broken line to emission. The small steps in JEPDS arise from the unit step function θ appearing in equation (5). At these steps only, energy and momentum are both conserved and a scattering event actually takes place. Physically, the occurrence of a step signals the disappearance of a phonon mode which can no longer contribute to a scattering event because of the requirement of simultaneous energy and momentum conservation as embodied in the unit step function θ.

In figure 3, there is a 'dead band' around the initial energy where $\text{JEPDS}^{\pm}$ is zero. This region obviously corresponds to quasi-elastic scattering, i.e. the case where the final-state

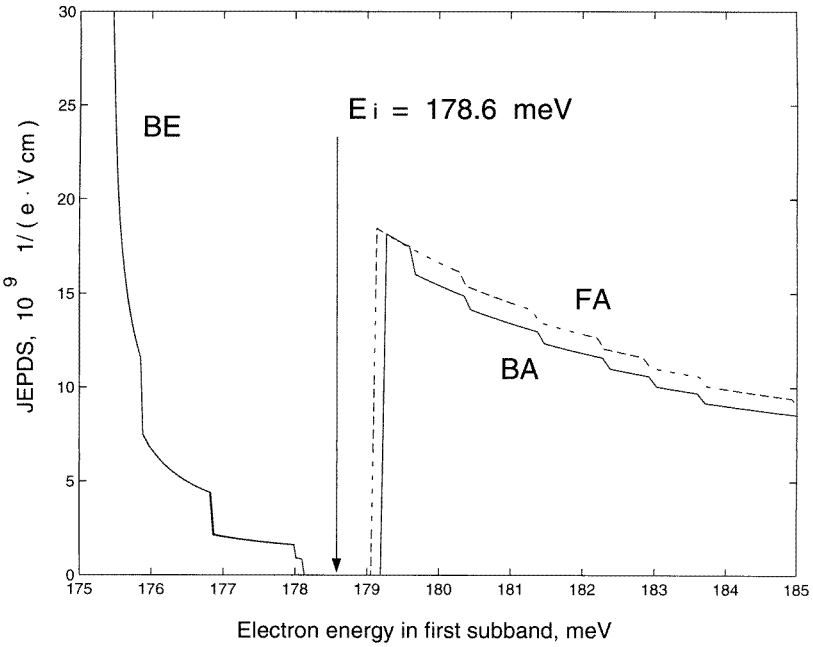

Figure 3. The joint electron–phonon density of (final) states (JEPDS$^{\pm}$) as 'seen' by an electron with energy $E = 178.6$ meV in the first subband of a GaAs quantum wire with cross-section 28.3 Å $\times$ 56.6 Å at zero magnetic field. The lattice temperature is 77 K and only intra-subband scattering has been considered. Energies below 178.6 meV correspond to backward emission (there is no forward emission in intra-band scattering). Energies above 178.6 meV correspond to absorption. The solid line is for backward absorption and the broken line for forward absorption.

energy is close to the initial-state energy. For intraband transitions, quasi-elastic events would require almost zero-energy phonons with non-zero wave vectors. Such phonons do not exist. Consequently, the JEPDS vanishes in this band.

In figures 4(a)–4(c), we plot the scattering rate $1/\tau(E_1)$, the momentum relaxation rate $1/\tau_m(E_1)$, and the energy relaxation rate $1/\tau_E(E_1)$ versus an electron's initial-state energy E_1 for deformation potential (non-polar acoustic phonon) scattering. The electron's initial state is in the first subband while the final state can be in any subband that is accessible up to the maximum initial energy considered plus a phonon energy. The lattice temperature is assumed to be 77 K and the quantum wire has a width of 500 Å and a thickness of 40 Å. The rates are plotted for two different values of the magnetic field: 0 and 10 T.

In figure 4, there are two very important features. First, the scattering rate calculated with *confined* acoustic phonons is, on average, *four* to *five* orders of magnitude higher than that calculated assuming *bulk* acoustic phonon modes [6]. This feature was also observed in reference [8]. As a result, the momentum and energy relaxation rates are also about five orders of magnitude higher than those calculated assuming bulk phonons [13]. Second, a magnetic field suppresses all relaxation rates associated with deformation potential interaction. The origin of this suppression is examined below.

A magnetic field has four major effects on electron–phonon interaction: (i) it suppresses backscattering [5, 6, 11] by spatially separating forward- and backward-travelling electron states, (ii) it suppresses inter-subband scattering by increasing the energy separation between the subbands (higher-energy phonons are required when the subband separation increases,

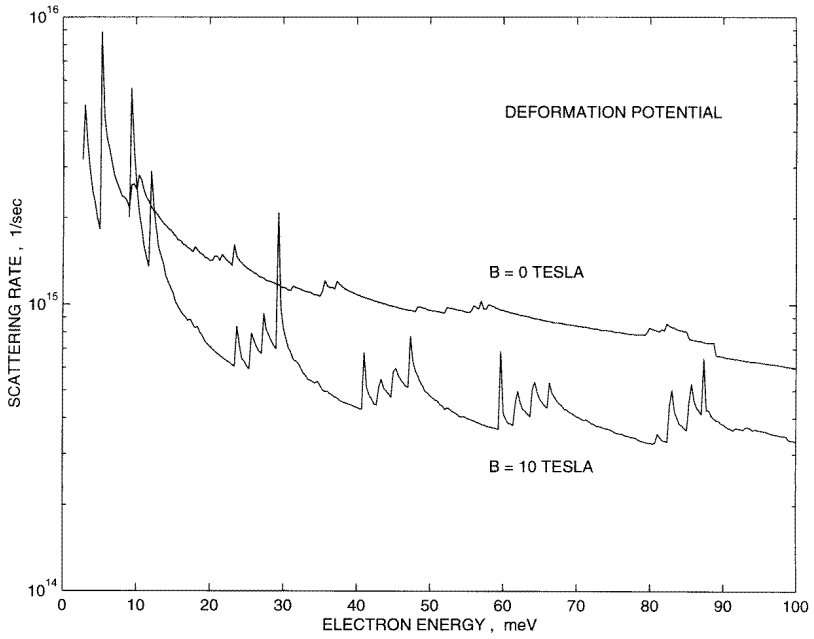

(a)

Figure 4. (a) The scattering rate $1/\tau(E_1)$ for an electron in the first subband versus the initial electron energy E_1. The rates are calculated for deformation potential interaction in a wire of width 500 Å and thickness 40 Å. The results are shown for two different values of the magnetic flux density: 0 and 10 T. The lattice temperature is 77 K. (b) The momentum relaxation rate $1/\tau_m(E_1)$ for an electron in the first subband versus the initial energy E_1. The rates are calculated for deformation potential interaction in a wire of width 500 Å and thickness 40 Å. The results are shown for two different values of the magnetic flux density: 0 and 10 T. The lattice temperature is 77 K. (c) The *magnitude* of the energy relaxation rate $1/\tau_E(E_1)$ for an electron in the first subband versus the initial energy E_1. The rates are calculated for deformation potential interaction in a wire of width 500 Å and thickness 40 Å. The results are shown for two different values of the magnetic flux density: 0 and 10 T. The lattice temperature is 77 K. The broken lines correspond to a *negative* energy relaxation rate and the solid lines to a *positive* energy relaxation rate. (d) The three constituents of the momentum relaxation rate $1/\tau_m(E_1)$ (backward emission, backward absorption, and forward absorption) are plotted as functions of the initial electron energy E_1 for a magnetic field of 0 T. The scattering is due to deformation potential interaction. There is no constituent due to forward emission since that is forbidden when the initial state of the electron is in the lowest subband. (e) The three constituents of the momentum relaxation rate $1/\tau_m(E_1)$ (backward emission, backward absorption, and forward absorption) are plotted as functions of the initial electron energy E_1 for a magnetic field of 10 T. The scattering is due to deformation potential interaction. There is no constituent due to forward emission since that is forbidden when the initial state of the electron is in the lowest subband. (f) The deformation scattering potential as a function of the wire width and phonon wave vector in a quantum wire of width 500 Å and thickness 40 Å.

and such phonons are rarer since the equilibrium phonon occupation factor obeys the Bose–Einstein distribution), (iii) it increases interface phonon scattering (electrons are pushed towards the edges of the wire by the Lorentz force and interact more strongly with interface phonons) [5], and (iv) it opens up new scattering channels and thus increases the total scattering rate [5]. This happens since a magnetic field skews the electron wave functions towards an edge of the wire and thus alters their parity. Therefore, transitions that are

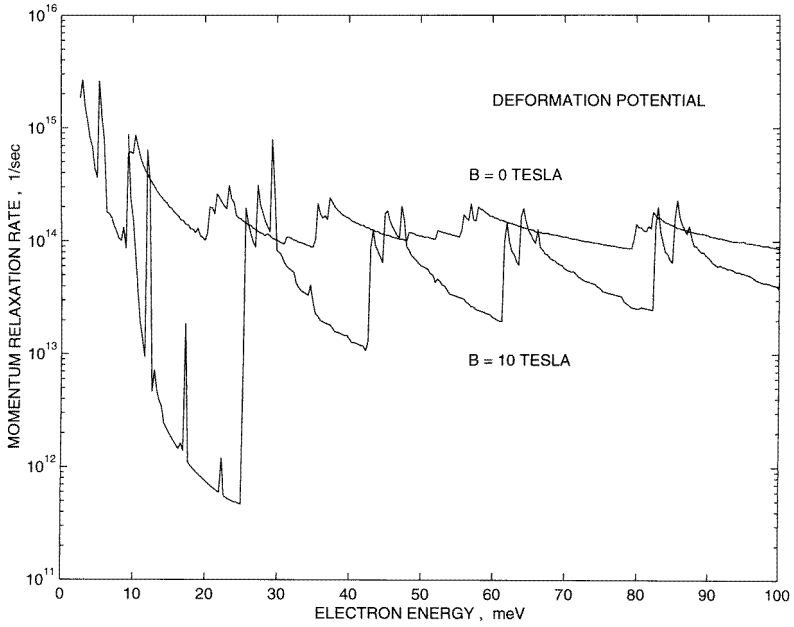

(b)

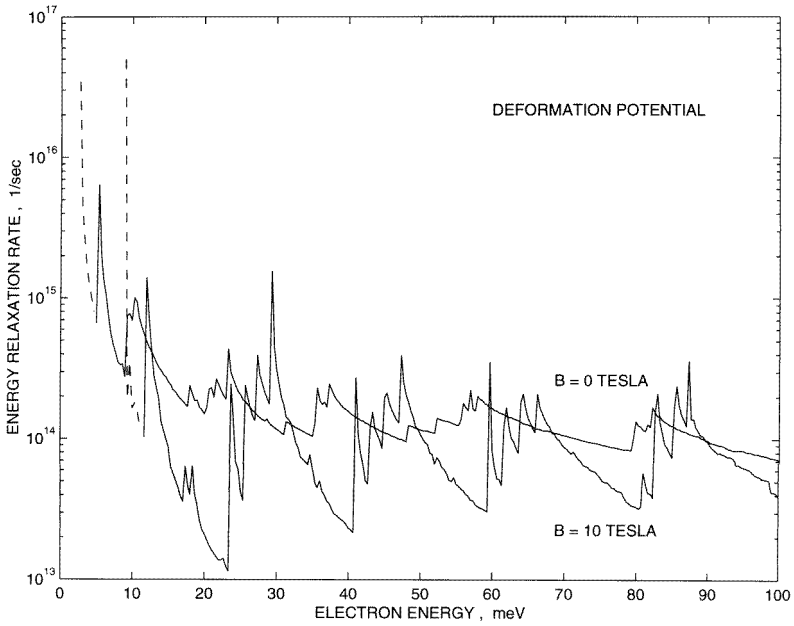

(c)

Figure 4. (Continued)

forbidden in the absence of a magnetic field (from parity considerations) are no longer forbidden [5].

Whether any particular relaxation rate actually increases or decreases in the presence of

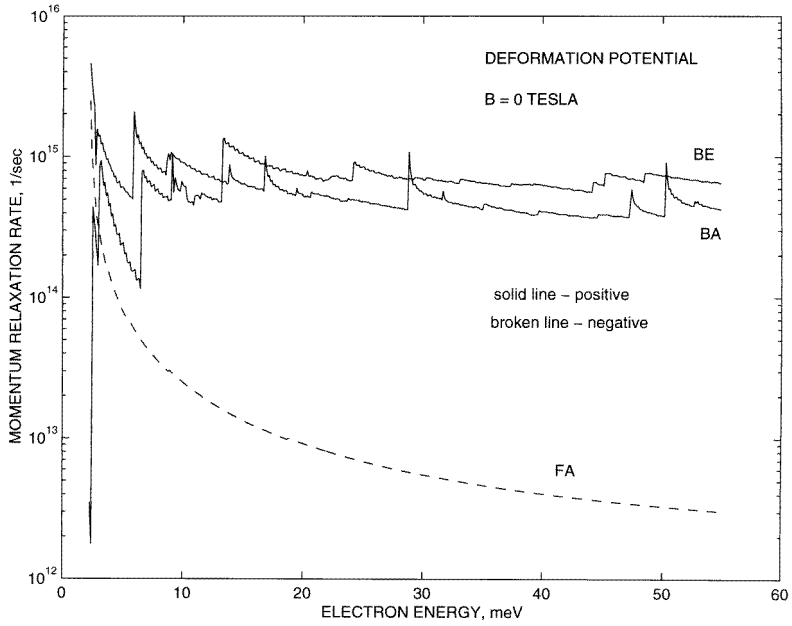

(d)

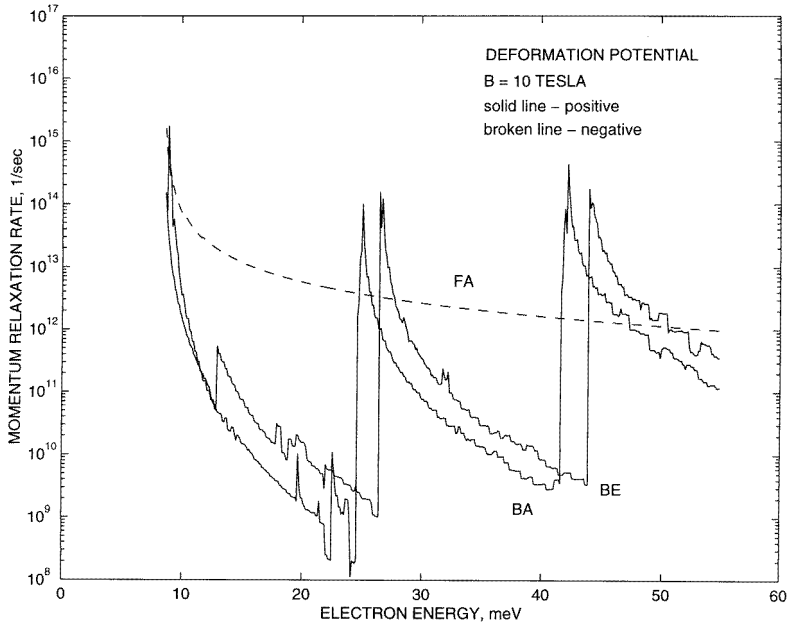

(e)

Figure 4. (Continued)

a magnetic field depends on the relative importance of the above four factors. In figure 4, we see that the deformation potential scattering rate (as well as the associated momentum and energy relaxation rates) decreases significantly in a magnetic flux density of 10 T. This

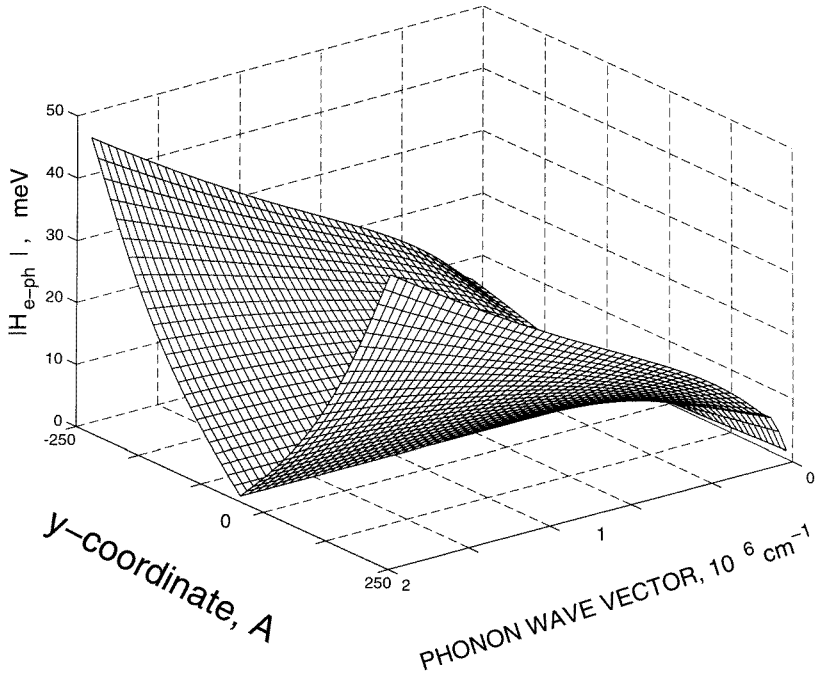

(f)

Figure 4. (Continued)

happens because suppression of backscattering is the predominant effect. In the absence of a magnetic field, backscattering is the principal mechanism for deformation potential scattering and it decreases significantly in a magnetic field [11]. Consequently, all relaxation rates drop. Suppression of backscattering has the most serious effect on the momentum relaxation rate since large momentum changes are caused by backscattering events rather than forward-scattering events. To demonstrate the suppression of backscattering in a magnetic field, we have plotted the rates for backward emission and absorption as well as forward absorption separately in figures 4(d) and 4(e). There is no forward emission since the initial state of the electron is in the lowest subband. In figure 4(d), no magnetic field is present while in figure 4(e) a magnetic flux density of 10 T is applied. Note that, by our definition, all forward-scattering events will have a negative momentum relaxation rate (since the momentum increases after scattering) while all backscattering events will have a positive momentum relaxation rate. In the absence of a magnetic field, backward emission is dominant in momentum relaxation and it decreases by five orders of magnitude when a magnetic flux density of 10 T is applied. Consequently, the overall momentum relaxation rate decreases and the mobility should increase.

The two factors that increase scattering in a magnetic field (interface phonons and the opening of new scattering channels) [5] are not that important for deformation potential scattering. To show why increased interface phonon interaction (due to the Lorentz force pushing electrons closer to the interface) is not important, we have plotted in figure 4(f) the magnitude of the deformation scattering potential as a function of the coordinate along the wire width and the phonon wave vector for the lowest phonon mode. Note that the scattering potential peaks at the edges of the wire ($y = \pm$ 250 Å), and so edge (or interface)

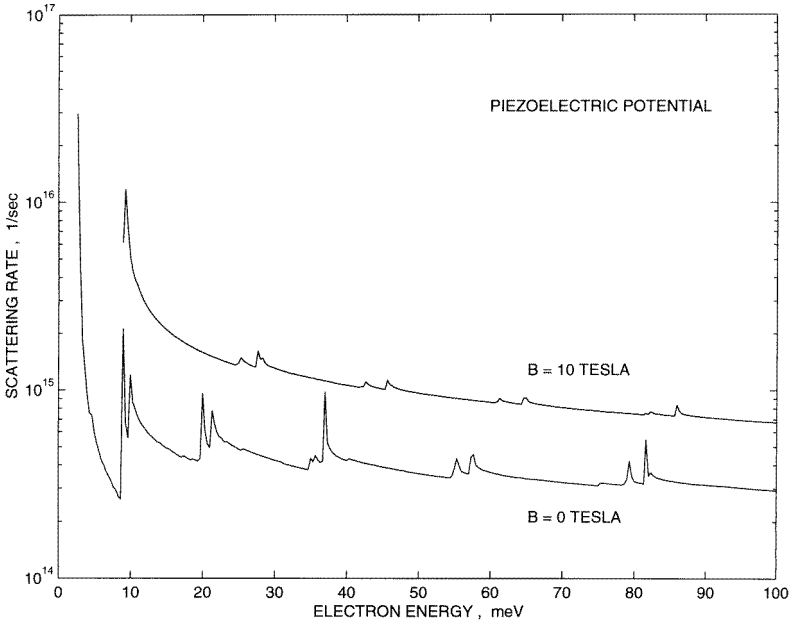

(a)

Figure 5. (a) The scattering rate $1/\tau(E_1)$ for an electron in the first subband versus the initial energy E_1. The rates are calculated for piezoelectric potential interaction in a wire of width 500 Å and thickness 40 Å. The results are shown for two different values of the magnetic flux density: 0 and 10 T. The lattice temperature is 77 K. (b) The momentum relaxation rate $1/\tau_m(E_1)$ for an electron in the first subband versus the initial energy E_1. The rates are calculated for piezoelectric potential interaction in a wire of width 500 Å and thickness 40 Å. The results are shown for two different values of the magnetic flux density: 0 and 10 T. The lattice temperature is 77 K. (c) The energy relaxation rate $1/\tau_E(E_1)$ for an electron in the first subband versus the initial energy E_1. The rates are calculated for piezoelectric potential interaction in a wire of width 500 Å and thickness 40 Å. The results are shown for two different values of the magnetic flux density: 0 and 10 T. The lattice temperature is 77 K. The two insets show regions where the energy relaxation rate is negative. Because of the very narrow widths of these regions, they are shown on expanded scales in the insets. (d) The piezoelectric scattering potential as a function of the wire width and phonon wave vector in a quantum wire of width 500 Å and thickness 40 Å.

phonons should be important. Therefore, at first glance, one would expect scattering to increase in a magnetic field since the electrons will be pushed towards the wire interfaces by the Lorentz force. However, the interface scattering potential is large only for phonons with a large wave vectors. Such phonons would tend to induce backscattering with large momentum change rather than forward scattering with a small momentum change. Thus, interface phonon interaction is primarily backscattering and that is suppressed by a magnetic field. As a result, any increase in interface phonon scattering is more than offset by the concomitant suppression of backscattering, so that the total scattering rate decreases in a magnetic field.

In figure 4(c), we see that the energy relaxation rate is negative at the lowest energies because absorption exceeds emission. At these very low energies, acoustic phonon emission is blocked by the rules of energy conservation for all but the lowest one or two confined phonon modes. As a result, absorption dominates. Note that *confined* acoustic phonons

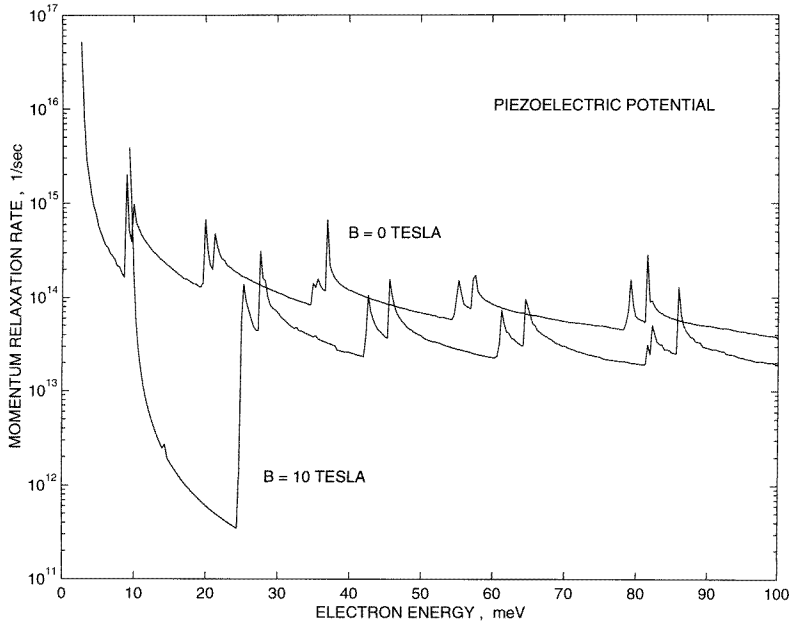

(b)

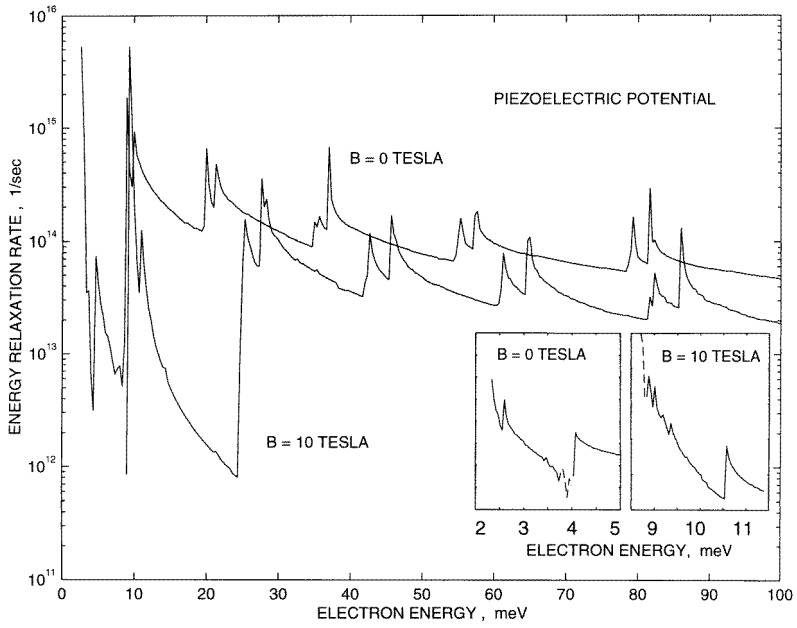

(c)

Figure 5. (Continued)

(except those in the lowest one or two modes) [11] have non-zero energy at all wave vectors unlike bulk acoustic phonons. Consequently, there is a finite *threshold energy* for the emission of confined acoustic phonons in all but the lowest one or two modes. This

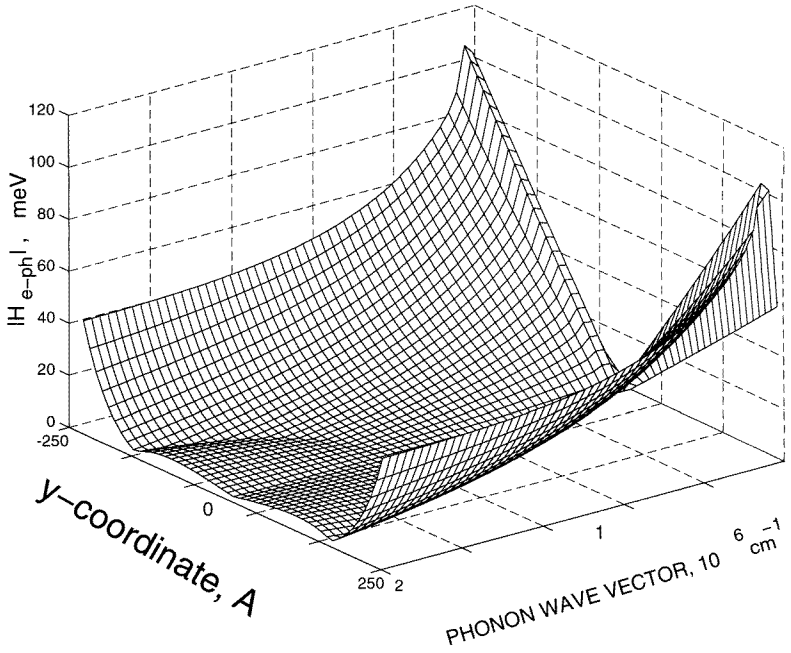

(d)

Figure 5. (Continued)

threshold is obviously different for different phonon modes. Whenever the electron energy is so low that it is below the thresholds for most phonon modes, absorption exceeds emission and causes the energy relaxation rate to be negative.

A negative energy relaxation rate can cause very efficient *transient* electron heating. If the electron distribution function resides in the energy interval of the negative energy relaxation rate, the distribution will be heated rapidly and then spread into regions of positive relaxation rate. Thereupon the distribution will cool and gradually reach a steady state. Once a steady state is reached, the principle of detailed balance will ensure that the overall absorption will equal the overall emission. All that the negative relaxation rate does is to speed up the onset of steady-state conditions. Thus the response of the system to an external electric field is faster. The negative relaxation rate will also cause a more pronounced velocity overshoot, since the latter is caused by a difference between the momentum and energy relaxation rates.

Note that a magnetic field decreases the energy relaxation rate by suppressing back-scattering.

In figures 5(a)–5(c), we have plotted the scattering rate, the momentum relaxation rate, and the energy relaxation rate associated with piezoelectric potential interaction at a lattice temperature of 77 K. The rates are plotted for magnetic flux densities of 0 and 10 T.

Figure 5(a) shows that the piezoelectric scattering rate goes up in a magnetic field. This happens because (i) forward scattering increases in a magnetic field, and (ii) forward scattering dominates over backward scattering, and hence even if the latter is suppressed by a magnetic field, the total scattering rate still increases. To demonstrate this, we have plotted in figure 5(d) the magnitude of the piezoelectric scattering potential as a function of the coordinate along the wire width and the phonon wave vector for the lowest phonon

mode. Note that the scattering potential peaks at the edges of the wire ($y = \pm 250$ Å), and so interface phonons are important. However, unlike in the case of deformation potential scattering, the piezoelectric scattering potential is larger at smaller phonon wave vectors. Thus, forward-scattering events that involve small momentum changes are preferred over backward-scattering events that cause large momentum changes. As a result forward scattering dominates. Since forward scattering is not suppressed by a magnetic field, it does not decrease, but rather, a magnetic field pushes electrons towards the wire interfaces and increases the forward scattering due to the closer proximity of electrons to interface phonons. Thus the total scattering rate goes up when a magnetic field is applied. This explains the trend seen in figure 5(a).

The momentum relaxation rate, on the other hand, is still dominated by backscattering since the latter causes much larger momentum changes than forward scattering which involves small-wave-vector phonons. Insofar as backscattering is always suppressed by a magnetic field [5, 6, 11], the momentum relaxation rate drops when a flux density of 10 T in applied. This is evident is figure 5(b).

Finally, in figure 5(c), we plot the energy relaxation rates as a function of the electron energy. Again, the energy relaxation rate is negative over certain intervals of energy where absorption dominates over emission. However, these intervals are very narrow. The magnetic field affects the region of negative energy relaxation rate and tends to shift it to higher energies by altering the ratio of emission to absorption events. Thus the mobility, diffusion coefficient (which depends on the electron temperature), noise spectral density, and a host of other transport parameters can be 'tuned' using a magnetic field.

4. Conclusion

In conclusion, we have calculated the energy and momentum relaxation rates for confined electrons interacting with confined acoustic phonons in a quantum wire subjected to a magnetic field. We found that phonon confinement increases the momentum and energy relaxation rates by about five orders of magnitude, and this should have a profound effect on the mobility of carriers. We also found that the momentum relaxation rate is always suppressed by a magnetic field, although the scattering rate may increase or decrease depending on whether the interaction is polar or non-polar. Moreover, we found that the energy relaxation rate can be negative over finite intervals of energy. These are regions of highly efficient *transient* electron heating. The existence of such regions promotes velocity overshoot (which is also a transient phenomenon), since overshoot is caused by the difference between the momentum and energy relaxation rates. This has important device implications since in quantum wire transistors, the saturation drain current, the transconductance, and the unity-gain frequency can all be improved by promoting velocity overshoot in the channel.

Acknowledgment

This work was supported by the US Army Research Office.

References

[1] Briggs S and Leburton J P 1988 *Phys. Rev.* B **38** 8163
[2] Jovanovic D, Briggs S and Leburton J P 1990 *Phys. Rev.* B **42** 11 108
[3] Kim K W, Stroscio M A, Bhatt A, Mickevicius R and Mitin V V 1991 *J. Appl. Phys.* **70** 319
[4] Mori N, Momose H and Hamaguchi C 1992 *Phys. Rev.* B **45** 4536

[5] Telang N and Bandyopadhyay S 1993 *Phys. Rev.* B **48** 18 002
[6] Telang N and Bandyopadhyay S 1993 *Appl. Phys. Lett.* **62** 3161
[7] Masale M and Constantinou N C 1993 *Phys. Rev.* B **48** 11 928
[8] SeGi Yu, Kim K W, Stroscio M A, Iafrate G J and Ballato A 1994 *Phys. Rev.* B **50** 1733
[9] Bannov N, Aristov V, Mitin V and Stroscio M A 1995 *Phys. Rev.* B **51** 9930
[10] Nishiguchi N, Ando Y and Wybourne M N 1997 *J. Phys.: Condens. Matter* **9** 5751
Nishiguchi N 1995 *Phys. Rev.* B **52** 5279
[11] Svizhenko A, Balandin A, Bandyopadhyay S and Stroscio M A 1998 *Phys. Rev.* B **57** 4687
[12] Chaudhuri S and Bandyopadhyay S 1992 *J. Appl. Phys.* **71** 3027
[13] Telang N and Bandyopadhyay S 1996 *Phys. Low Dimens. Struct.* **9+10** 63